

1 Probing initial and final state effects of heavy-ion collisions with
2 STAR experiment*

3 GAOGUO YAN (FOR THE STAR COLLABORATION)

4 Institute of Frontier and Interdisciplinary Science, Shandong University,
5 Qingdao, Shandong, 266237, China

6 *Received July 28, 2022*

7 Measurements of longitudinal flow decorrelation for charged particles
8 in Zr+Zr and Ru+Ru (isobar) collisions at $\sqrt{s_{\text{NN}}} = 200$ GeV and Au+Au
9 collisions at $\sqrt{s_{\text{NN}}} = 19.6, 27$ and 54.4 GeV using STAR detector are pre-
10 sented. The third order flow decorrelation is stronger than the second order.
11 The second order flow decorrelation shows a strong centrality dependence,
12 while the third order results show a weak dependence. Comparing with
13 Au+Au collisions at $\sqrt{s_{\text{NN}}} = 27$ and 54.4 GeV, both the second and third
14 order flow decorrelations show obvious energy dependence. In addition,
15 the correlation coefficient $\rho(v_n^2, [p_T])$ is also measured in Au+Au collisions
16 at $\sqrt{s_{\text{NN}}} = 19.6 - 200$ GeV. No obvious energy dependence is observed for
17 $\rho(v_n^2, [p_T])$. These results provide significant constraints on the initial-state
18 fluctuations.

19 **1. Introduction**

20 Heavy-ion collisions create a strongly coupled, hot and dense medium
21 known as a quark gluon plasma (QGP) whose space time evolution is de-
22 scribed by relativistic viscous hydrodynamic models. During its dynamical
23 evolution, the spatial anisotropy in the initial state geometry can transform
24 into the momentum anisotropy of final state particles because of large pres-
25 sure gradients. This anisotropy of final state particles can be characterized
26 by the Fourier expansion of final particles yield distribution in azimuthal
27 angle, $dN/d\phi \propto 1 + 2 \sum_n v_n \cos[n(\phi - \psi_n)]$, where v_n and ψ_n are the mag-
28 nitude and phase angle of anisotropic flow. In early days of flow studies,
29 we usually assume that initial state is smooth and flow is boost-invariant.
30 However, initial state fluctuations play an important role, for example, the
31 fluctuations of nucleon positions.

* Presented at 29th International Conference on Ultra-relativistic Nucleus-Nucleus Col-
lisions (Quark Matter 2022), Krakow, Poland

32 Recently, both theoretical models [1–3] and experiments [4–7] show that
 33 v_n and ψ_n can fluctuate along the longitudinal direction. Such decorrelation
 34 effects can be characterized by the factorization ratio $r_n(\eta)$ [4].

$$\begin{aligned} r_n(\eta) &= \frac{\langle q_n(-\eta)q_n^*(\eta_{ref}) \rangle}{\langle q_n(\eta)q_n^*(\eta_{ref}) \rangle}, \\ &= \frac{\langle v_n(-\eta)v_n(\eta_{ref}) \cos\{n[\psi_n(-\eta) - \psi_n(\eta_{ref})]\} \rangle}{\langle v_n(\eta)v_n(\eta_{ref}) \cos\{n[\psi_n(\eta) - \psi_n(\eta_{ref})]\} \rangle}, \end{aligned} \quad (1)$$

35 where $\langle \dots \rangle$ indicates an average over all events, $q_n(\eta)$ and $q_n(-\eta)$ are con-
 36 structed from charged tracks measured in Time Projection Chamber (TPC,
 37 $|\eta| < 1.0$) and $q_n(\eta_{ref})$ is constructed from Event Plane Detector (EPD,
 38 $2.1 < |\eta_{ref}| < 5.1$). The $r_n(\eta)$ measures relative fluctuations between for-
 39 ward ($+\eta$ range) and backward ($-\eta$ range) rapidities. In this proceedings,
 40 we present flow decorrelation results in Zr+Zr and Ru+Ru collisions at
 41 $\sqrt{s_{NN}} = 200$ GeV and Au+Au collisions at $\sqrt{s_{NN}} = 19.6, 27$ and 54.4 GeV
 42 using STAR detector to explore system size and energy dependence. The
 43 charged particles are required to have transverse momentum, $0.4 < p_T <$
 44 4.0 GeV/ c and pseudorapidity range, $|\eta| < 1.0$, except for 19.6 GeV with
 45 $|\eta| < 1.5$ because of using inner Time Projection Chamber (iTTPC). The
 46 systematic uncertainties are evaluated by using negative and positive tracks
 47 separately, and by varying track selections.

48 The shape and size of initial state fluctuations can contribute to the
 49 higher harmonics (v_n for $n=3,4,\dots$) and to the fluctuation of mean trans-
 50 verse momentum $[p_T]$ of final state particles, respectively. The $v_n - [p_T]$
 51 correlation can probe the correlation between shape and size in initial state.
 52 The Pearson correlation coefficient (PCC) [8] is used to indicate strength of
 53 $v_n - [p_T]$ correlation.

$$\rho(v_n^2, [p_T]) = \frac{cov(v_n^2, [p_T])}{\sqrt{var(v_n^2)}\sqrt{var([p_T])}}, \quad (2)$$

54 where $cov(v_n^2, [p_T])$ is the covariance between v_n^2 and $[p_T]$, and $var(v_n^2)$ and
 55 $var([p_T])$ are the variances of the v_n^2 and $[p_T]$ distributions, respectively.
 56 Experimental results can provide important constraints on models with the
 57 initial-state conditions [9, 10]. In this proceedings, we also present $v_n - [p_T]$
 58 correlation results in Au+Au collisions at $\sqrt{s_{NN}} = 19.6, 27, 54.4$ and 200
 59 GeV to probe its beam energies dependence.

60

2. Results and Discussions

61 Figures 1 and 2 show the $r_n(\eta)$ for $n = 2, 3$ in Zr+Zr and Ru+Ru
 62 collisions at $\sqrt{s_{NN}} = 200$ GeV in 0-10%, 10-40% and 40-80% centralities.

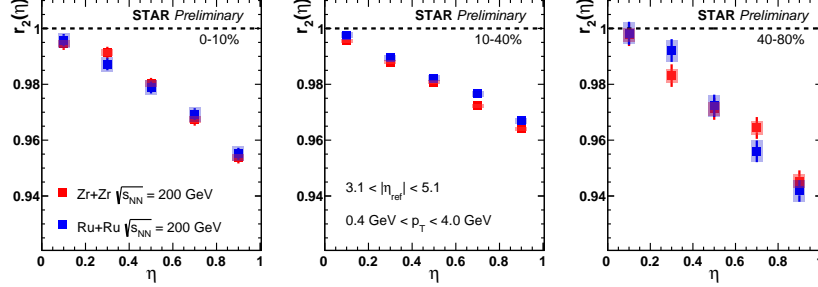


Fig. 1. The factorization ratio $r_2(\eta)$ in Zr+Zr (red squares) and Ru+Ru (blue squares) collisions at $\sqrt{s_{\text{NN}}} = 200$ GeV in three centralities. The error bars and shaded boxes represent statistical and systematic uncertainties, respectively

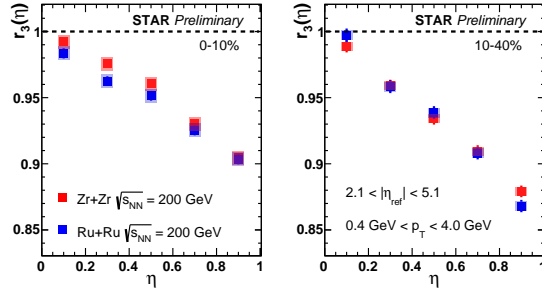


Fig. 2. The factorization ratio $r_3(\eta)$ in Zr+Zr (red squares) and Ru+Ru (blue squares) collisions at $\sqrt{s_{\text{NN}}} = 200$ GeV in two centralities. The error bars and shaded boxes represent statistical and systematic uncertainties, respectively

63 The $r_n(\eta)$ results between Zr+Zr and Ru+Ru collisions are consistent within
 64 uncertainties. The value of $r_n(\eta)$ decreases linearly with increasing η . The
 65 values of $r_3(\eta)$ are smaller than $r_2(\eta)$, implying a stronger flow decorrelation
 66 for higher order harmonics. The second order flow decorrelation becomes
 67 weak first and then strong as we move from central to peripheral collisions.
 68 Such a dependence is the result of a strong centrality dependence of v_2 which
 69 is dominated by initial elliptic geometry. On the other hand, no obvious
 70 centrality dependence for the third order flow decorrelation is observed since
 71 the third order flow is driven by initial fluctuations.

72 Figures 3 and 4 show the $r_n(\eta)$ for $n = 2, 3$ in Au+Au collisions at $\sqrt{s_{\text{NN}}}$
 73 $= 19.6, 27$ and 54.4 GeV in 0-10%, 10-40% and 40-80% centralities. For each
 74 energy, the longitudinal flow decorrelation depends on the harmonic order
 75 n and collision centrality and decreases linearly with η as observed in isobar
 76 collisions. The slope of $r_2(\eta)$ at 27 GeV is stronger than that at 54.4 GeV,

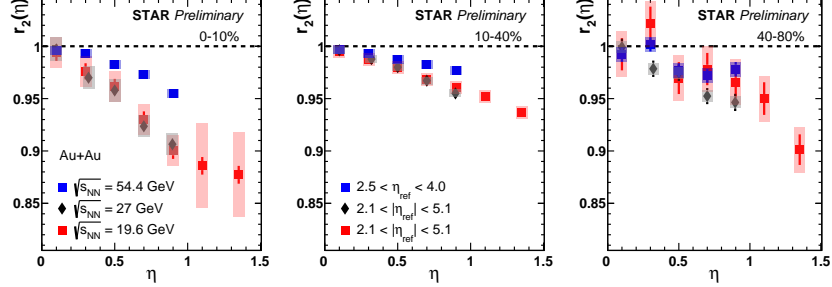


Fig. 3. The factorization ratio $r_2(\eta)$ in Au+Au collisions at $\sqrt{s_{\text{NN}}} = 19.6$ GeV (red squares), 27 (black diamonds) and 54.4 (blue squares) in three centralities. The error bars and shaded boxes represent statistical and systematic uncertainties, respectively

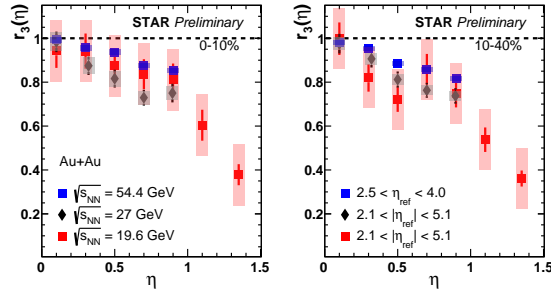


Fig. 4. The factorization ratio $r_3(\eta)$ in Au+Au collisions at $\sqrt{s_{\text{NN}}} = 19.6$ GeV (red squares), 27 (black diamonds) and 54.4 (blue squares) in two centralities. The error bars and shaded boxes represent statistical and systematic uncertainties, respectively

77 indicating that lower energy collisions has large decorrelation. This effect
 78 is similar to observations from the LHC results [5], which indicates that
 79 lower energy collisions become less boost-invariant along the longitudinal
 80 direction. However, there is no obvious difference between 19.6 and 27 GeV
 81 which might be due to their small energy difference. No solid conclusion of
 82 energy dependence can be drawn for $r_3(\eta)$ due to statistical limitation.

83 Figure 5 shows beam energy dependence of $\text{var}(v_2^2)$, c_k , $\text{cov}(v_2^2, [p_T])$ and
 84 $\rho(v_2^2, [p_T])$ in different centralities. The $\text{var}(v_2^2)$, c_k and $\text{cov}(v_2^2, [p_T])$ decrease
 85 with beam energy due to larger contribution from average p_T change. The
 86 $\rho(v_2^2, [p_T])$ is sensitive to initial fluctuations and shows a hint of beam energy
 87 dependence, which indicates stronger correlation at lower energy.

88 Figure 6 compares $\text{var}(v_3^2)$, c_k , $\text{cov}(v_3^2, [p_T])$ and $\rho(v_3^2, [p_T])$ for Au+Au

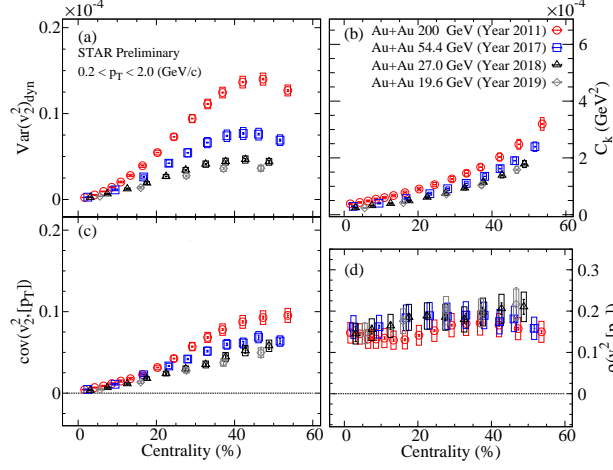


Fig. 5. The centrality dependence of $\text{var}(v_2^2)$ (a), c_k (b), $\text{cov}(v_2^2, [p_T])$ (c) and $\rho(v_2^2, [p_T])$ (d) for Au+Au collisions at $\sqrt{s_{\text{NN}}} = 19.6, 27, 54.4$ and 200 GeV.

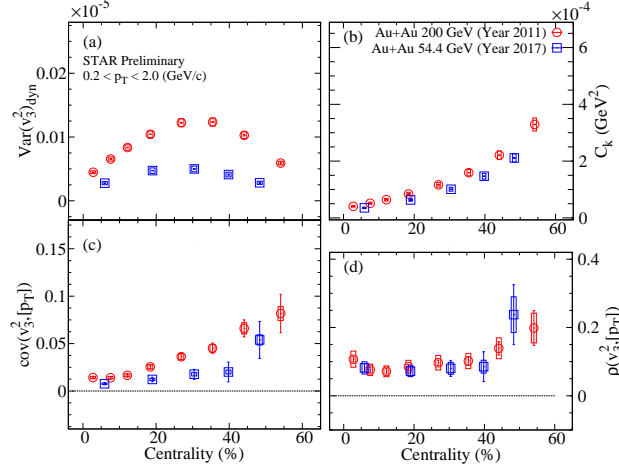


Fig. 6. The centrality dependence of $\text{var}(v_3^2)$ (a), c_k (b), $\text{cov}(v_3^2, [p_T])$ (c) and $\rho(v_3^2, [p_T])$ (d) for Au+Au collisions at $\sqrt{s_{\text{NN}}} = 54.4$ and 200 GeV.

89 collisions between $\sqrt{s_{\text{NN}}} = 200$ and 54.4 GeV. Similarly, the $\text{var}(v_3^2)$, c_k and
 90 $\text{cov}(v_3^2, [p_T])$ decrease with beam energy. However, the $\rho(v_3^2, [p_T])$ shows no
 91 clear energy dependence which demonstrates similar initial fluctuations in
 92 $\sqrt{s_{\text{NN}}} = 200$ and 54.4 GeV.

3. Conclusion

93
 94 The longitudinal flow decorrelation for charged particles was measured
 95 in Zr+Zr and Ru+Ru collisions at $\sqrt{s_{\text{NN}}} = 200$ GeV and Au+Au collisions
 96 at $\sqrt{s_{\text{NN}}} = 19.6, 27$ and 54.4 GeV. The factorization ratio $r_n(\eta)$ decreases
 97 linearly with increasing η showing that flow decorrelation is stronger at
 98 larger η separation between the two particles. For $n = 2$, the effect is smallest
 99 in 10-40% centrality and increases in 0-10% and 40-80% centralities. For $n =$
 100 3 , there is no obvious centrality dependence. Comparisons with $\sqrt{s_{\text{NN}}} = 27$
 101 and 54.4 GeV show strong energy dependence. In addition, the correlation
 102 coefficient $\rho(v_n^2, [p_T])$ was also measured in Au+Au collisions at $\sqrt{s_{\text{NN}}} =$
 103 $19.6, 27, 54.4$ and 200 GeV. No obvious energy dependence is observed for
 104 the results. These results provide new insights for three-dimensional initial
 105 state and important input for theoretical models.

REFERENCES

- 106 [1] P. Bozek, W. Broniowski, and J. Moreira, Torqued Fireballs in Relativistic
 107 Heavy-Ion Collisions, *Phys. Rev. C* 83, 034911 (2011).
 108 [2] J. Jia and P. Huo, Forward-Backward Eccentricity and Participant-Plane
 109 Angle Fluctuations and Their Influences on Longitudinal Dynamics of Col-
 110 lective Flow, *Phys. Rev. C* 90, 034915 (2014).
 111 [3] L.-G. Pang and et al. , Decorrelation of Anisotropic Flow along the Longitu-
 112 dinal Direction, *Eur. Phys. J. A* 52, 97 (2016).
 113 [4] CMS Collaboration, Evidence for Transverse Momentum and Pseudorapidity
 114 Dependent Event Plane Fluctuations in PbPb and pPb Collisions, *Phys. Rev.*
 115 *C* 92, 034911 (2015).
 116 [5] ATLAS Collaboration, Measurement of Longitudinal Flow De-Correlations
 117 in Pb+Pb Collisions at $\sqrt{s_{\text{NN}}} = 2.76$ TeV and 5.02 TeV with the ATLAS
 118 Detector, *Eur. Phys. J. C* 78, 142 (2018).
 119 [6] ATLAS Collaboration, Longitudinal Flow Decorrelations in Xe+Xe Colli-
 120 sions at $\sqrt{s_{\text{NN}}} = 5.44$ TeV with the ATLAS Detector, *Phys. Rev. Lett.* 126,
 121 122301 (2021).
 122 [7] M. Nie, Energy Dependence of Longitudinal Flow Decorrelation from STAR,
 123 *Nucl. Phys. A* 1005, 121783 (2021).
 124 [8] P. Bozek, Transverse Momentum-Flow Correlations in Relativistic Heavy-Ion
 125 Collisions, *Phys. Rev. C* 93, 044908 (2016).
 126 [9] ATLAS Collaboration, Measurement of Flow Harmonics Correlations with
 127 Mean Transverse Momentum in Lead–Lead and Proton–Lead Collisions at
 128 $\sqrt{s_{\text{NN}}} = 5.02$ TeV with the ATLAS Detector, *Eur. Phys. J. C* 79, 985 (2019).
 129 [10] N. Magdy and et al., Model Study of the Energy Dependence of the Cor-
 130 relation between Anisotropic Flow and the Mean Transverse Momentum in
 131 Au+Au Collisions, *Phys. Rev. C* 105, 044901 (2022).